

# Single-shot Complete Spatiotemporal Measurement of Complex Ultrashort Laser Pulses

Zhe Guang

School of Physics, Georgia Institute of Technology, 837 State Street, Atlanta, Georgia 30332, USA  
Email Address: zguang3@gatech.edu

## 1. Literature Review

### I. Challenge to Measure Ultrashort Laser Pulses

The birth of laser in the 1960s opened up a new era for optics. Many interesting laser applications arose ever since in subjects like nonlinear optics, holography, spectroscopy, and quantum optics [1-4]. Among those, ultrafast optics is an emerging area that frequently catches people's attention. Ultrafast optics deals with short pulses in time scale ranging from picosecond down to attosecond, generated from all variety of pulsed laser systems by approaches like mode-locking and Q-switching. The ultrashort temporal width, together with the resulting ultrahigh peak intensity and ultrabroad spectral bandwidth, of the generated pulses leads to special academic interests in studying ultrafast phenomena, nonlinear optical effects, broadband spectroscopy, and so on [5-7].

For better manipulation, after their generation, ultrashort pulses need to be characterized, to know their detailed pulse shape, or at least, to be proven ultrashort. But, as ultrashort pulses vary a lot faster (typically  $\sim 10^{-15}$ s) than the electronic monitoring speed (typically  $\sim 10^{-10}$ s), getting knowledge of their temporal *intensity* information keeps being challenging [8]. Moreover, as the *intensity* vs. time only represents half the information of a pulse, the other half, i.e. the *phase* variations, is generally blind to electronic detection devices. The "missing" phase information, however, is in many ways more important than the intensity: the temporal phase tells us how fast electrical field is oscillating, and the spectral phase describes the pulse's frequency evolution vs. time. As a result, people have been developing *optical* techniques that capture the ultrafast variations both in intensity and phase, temporally or spectrally:

$$E(t) = \text{Re}\{\sqrt{I(t)} \exp[i(\omega_0 t - \phi(t))]\}$$

$$\tilde{E}(\omega) = \sqrt{S(\omega)} \exp[-i\varphi(\omega)]$$

$$\tilde{E}(\omega) = FT\{E(t)\}, \quad E(t) = IFT\{\tilde{E}(\omega)\}$$

where  $I(t)$  and  $\phi(t)$  are temporal intensity and temporal phase, and  $S(\omega)$  and  $\varphi(\omega)$  are spectral intensity (also known as spectrum) and spectral phase. The temporal and spectral fields,  $E(t)$  and  $\tilde{E}(\omega)$ , are related by Fourier transforms.

Two decades ago, our group developed the first technique for the complete temporal measurement of ultrashort laser pulses, Frequency-Resolved Optical Gating (FROG) [8,9], which measures the pulse intensity and phase vs. time and frequency without the need for a previously characterized reference pulse. FROG is now in use in most ultrafast-optics labs around the world. It can measure pulses of almost any wavelength [10,11] and pulse length from nanoseconds [12] to attoseconds [13].

FROG, however, is designed for measuring fairly simple, spatially uniform pulses from lasers, without much characterization on their spatial profile. In fact, as most objects in our universe are spatially complex, any light emerging from them is necessarily also. Thus, temporal and spatial complexities of light both contain vast amount of information, which calls for techniques that more completely characterize them.

Over the centuries, much effort has been devoted to measuring light intensity's spatial variations, but almost always averaging over its fast temporal variations. Great success has been achieved by recording time-integrated spatial intensity, as the history of photography attests. Also, spatial-phase measurements have been performed for narrowband beams (holography). However, ultrashort pulses' temporal variations are rarely the same from point to point in space, and, equivalently, their spatial variations are rarely the same from point to point in time. These variations are usually called *spatiotemporal couplings* (STC) or *distortions*, depending on whether they are useful or problematic for a given application. Though they are very important pulse features, unfortunately, spatial measurements that average over time and temporal measurements that average over space do not measure them. Thus, the STCs essentially always go unmeasured, except for very slow variations cases.

As a result, our ultimate goal is to develop a technique to measure, for an arbitrary light wave and by making no assumptions, the complete electric field of light, that is, its intensity  $I$  and phase  $\phi$  vs. space  $x$ ,  $y$ ,  $z$  and time  $t$ :

$$E(x, y, z, t) = \text{Re}\{\sqrt{I(x, y, z, t)} \exp[i(\omega_0 t - \phi(x, y, z, t))]\}$$

or, equivalently, vs.  $x$ ,  $y$ ,  $z$  and frequency  $\omega$ :

$$\tilde{E}(x, y, z, \omega) = \sqrt{S(x, y, z, \omega)} \exp[-i\phi(x, y, z, \omega)]$$

Note that, for all quantities here, the spatial part and temporal/spectral part are not necessarily separable, e.g.,  $E(x, y, z, t) \neq E(x, y, z) \times E(t)$  or  $\tilde{E}(x, y, z, \omega) \neq \tilde{E}(x, y, z) \times \tilde{E}(\omega)$ . For each position, of course, the temporal and spectral fields are also related by Fourier transforms, in a similar form as before:

$$\tilde{E}(x, y, z, \omega) = FT\{E(x, y, z, t)\}, \quad E(x, y, z, t) = IFT\{\tilde{E}(x, y, z, \omega)\}$$

Once the electric field vs.  $x$ ,  $y$ , and  $t$  (or  $\omega$ ) is determined, its  $z$ -dependency could always be obtained by propagating the diffraction integral [2]. As a result, the  $z$ -dependencies in most expressions are ignored in this paper.

## II. Review of Spatiotemporal Pulse Measurement Techniques

As discussed above, ultrashort laser pulses have various applications in academia and industry. Most such applications operate best with a pulse that has stable and simple (or at least known) intensity and phase in both space and time. Unfortunately, ultrafast lasers suffer from an abundance of *spatiotemporal couplings*. Some spatiotemporal couplings are useful in such applications as coherent control, pulse compression, and nonlinear optics [14-18], but most are not. For example, in Kerr-lens mode locked lasers, the output mode size depends on frequency [19], and, even if it does not, it will at a focus. And since dispersive and focusing optics are ubiquitous in ultrafast laser systems, numerous additional spatiotemporal distortions, such as radial dispersion and chromatic aberration, often occur [20-23].

Furthermore, ultrashort pulses, especially amplified ones, have extremely high intensities, so significant intensity-related nonlinear-optical effects can distort pulses as they propagate through optics [24-28]. These latter distortions are particularly problematic because they vary from shot to shot when intensity fluctuations are present, and, in ultrahigh-intensity low-rep-rate systems, the shot-to-shot variations can be significant. As a result, a technique that can measure the complete spatiotemporal intensity-and-phase (electric field) of an ultrashort light pulse,  $E(x,y,t)$ , would be very useful, and, in particular, for high-intensity, low-rep-rate pulses, a *single-shot* technique is essential.

Unfortunately, complete spatiotemporal characterization of ultrashort laser pulses remains extremely challenging. As seen above, the temporally averaged spatial profiles obtained using simple cameras, or spatially averaged temporal profiles measured using methods like FROG are not sufficient to characterize the spatiotemporal pulses. Even so, single-shot versions of FROG and its simpler cousin, GRENOUILLE [29,30], have been managed to yield simple first-order spatiotemporal distortions, specifically, spatial chirp and pulse-front-tilt [31,32]. However, more powerful techniques are needed to completely characterize spatiotemporally complex pulses.

More recently, a number of techniques that yield partial solutions to the spatiotemporal-measurement problem have been proposed and demonstrated [33,34]. Beginning with methods that measure the temporal profile using a measured trace that is only one-dimensional (such as spectral interferometry), it is straightforward to extend the measurement using a standard two-dimensional camera to also include one spatial domain, i.e.  $E(x,t)$  or  $E(x,\omega)$  [35-41]. The resulting measurement, however, remains incomplete in space (either cropping or averaging over the missed spatial dimension), so assumptions must be made about the spatial homogeneity or cylindrical symmetry—which may not be valid in practice. To obtain the additional dimension, one must scan over it spatially.

Other techniques use combinations of spatial and temporal measurements. Shackled FROG [42,43] and HAMSTER [44], are based on combining a Hartmann-Shack spatial sensor with a FROG apparatus. The Hartmann-Shack sensor yields the spatial wave-front and amplitude information, and a FROG measurement of the central part (or anywhere else that contains all frequency components) stitches together the results. These methods are limited, however, because they must assume the same spatial phase for each monochromatic component [42] or must scan over all frequencies [45]; otherwise, the obtained information is spatially incomplete [43].

It is helpful to generate a spatiotemporally known reference pulse or train of pulses to assist with the measurement. This can be accomplished by spatially filtering a pulse to achieve a spatially simple (known) beam and then measuring the resulting essentially spatially uniform field vs. time [46,47]. Most such methods with known reference pulse still involve scanning in the spatial dimension(s), and the most popular include SEA TADPOLE [48] and STARFISH [49]. These methods can measure pulses completely in space and time, i.e.  $E(x,y,t)$ . As both of the above methods scan fibers to probe pulses, they are inherently alignment-free and have high spatial resolution. However, as with all spatial or spectral scanning techniques [50-53], such methods require many shots, rendering them inapplicable for unstable or low-repetition-rate pulse trains. This is unfortunate, as these pulses are usually of greater interest, especially amplified pulses from complex systems that also more often incur nonlinear-optical spatiotemporal distortions.

### III. Review of STRIPED FISH: the Previous Work

To solve the above problems, we recently introduced a single-shot technique for complete spatiotemporal pulse measurement (vs.  $x$ ,  $y$ , and  $t$ ). It is called Spatially and Temporally Resolved Intensity and Phase Evaluation Device: Full Information from a Single Hologram (STRIPED FISH) [54]. It comprises a very simple setup of only a coarse two-dimensional diffractive optical element (DOE), an interference band-pass filter (IBPF), imaging optics, and a camera (see Fig. 1). It uses a previously spatially smoothed and temporally characterized reference pulse, accomplished at an earlier point using a spatial filter and a FROG measurement. The pulse to be measured and the known reference pulse cross at a small vertical angle on the DOE, which simultaneously generates multiple divergent pairs of beams at different angles. The DOE is also rotated slightly, so the horizontal propagation angle is different for each beam pair. Because the IBPF's transmission center wavelength varies with horizontal incidence angle, it then wavelength-filters each pair of beams to be essentially monochromatic and with different center wavelengths [55,56]. The beam pairs then overlap at the camera, generating an array of quasi-monochromatic holograms, each at a different wavelength. The spatiotemporal information of the unknown pulse is obtained from the multiple holograms and the knowledge of the reference pulse, yielding a complete measurement on a single camera frame and hence, if desired, on a single shot.

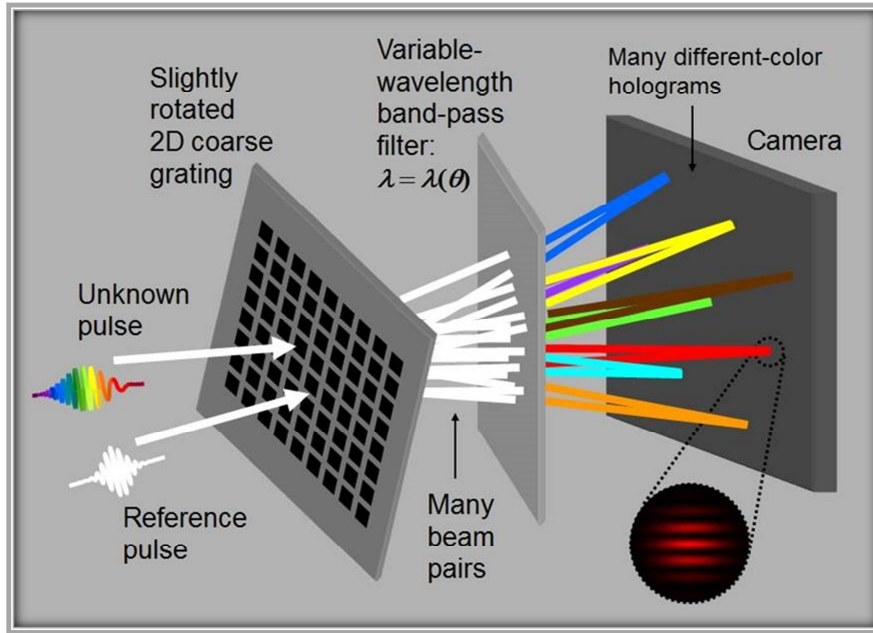


Figure 1. Conceptual schematic of STRIPED FISH.

To measure the unknown pulse, we first temporally characterize a spatially filtered simple pulse, as a spatiotemporally known reference,  $E_r(x,y,\omega)$ . This pulse then crosses with the unknown pulse,  $E_u(x,y,\omega)$ , at a small vertical angle  $\alpha$ , forming an interfering beam pair. By passing through the DOE and the IBPF, holograms of many different frequencies are generated. The interference of the reference and unknown pulses at each frequency is given by:

$$I(x, y, \omega) = |E_u(x, y, \omega)|^2 + |E_r(x, y, \omega)|^2 + E_u(x, y, \omega)E_r(x, y, \omega)^* \exp(+ik_y \sin(\alpha)) + E_r(x, y, \omega)E_u(x, y, \omega)^* \exp(-ik_y \sin(\alpha))$$

where the asterisk denotes the complex conjugate. Note that all amplitude and phase information of the unknown pulse is contained within the oscillating term  $E_u(x,y,\omega)E_r^*(x,y,\omega)\exp(+ik_y\sin(\alpha))$ , where the “carrier”  $\exp(+ik_y\sin(\alpha))$  is easily removed to retrieve the “envelope”  $E_u(x,y,\omega)E_r^*(x,y,\omega)$  by a Fourier-filtering algorithm [57]. Furthermore, because  $E_r(x,y,\omega)$  is known, the complex unknown spatio-spectral field  $E_u(x,y,\omega)$  is then obtained. By performing an inverse Fourier transform for each location, we obtain the unknown field in spatiotemporal domain,  $E_u(x,y,t)$ . To illustrate this, we demonstrate the retrieval of a positively chirped Gaussian pulse, following proper calibration parameters, from a simulated trace, as shown in Fig. 2.

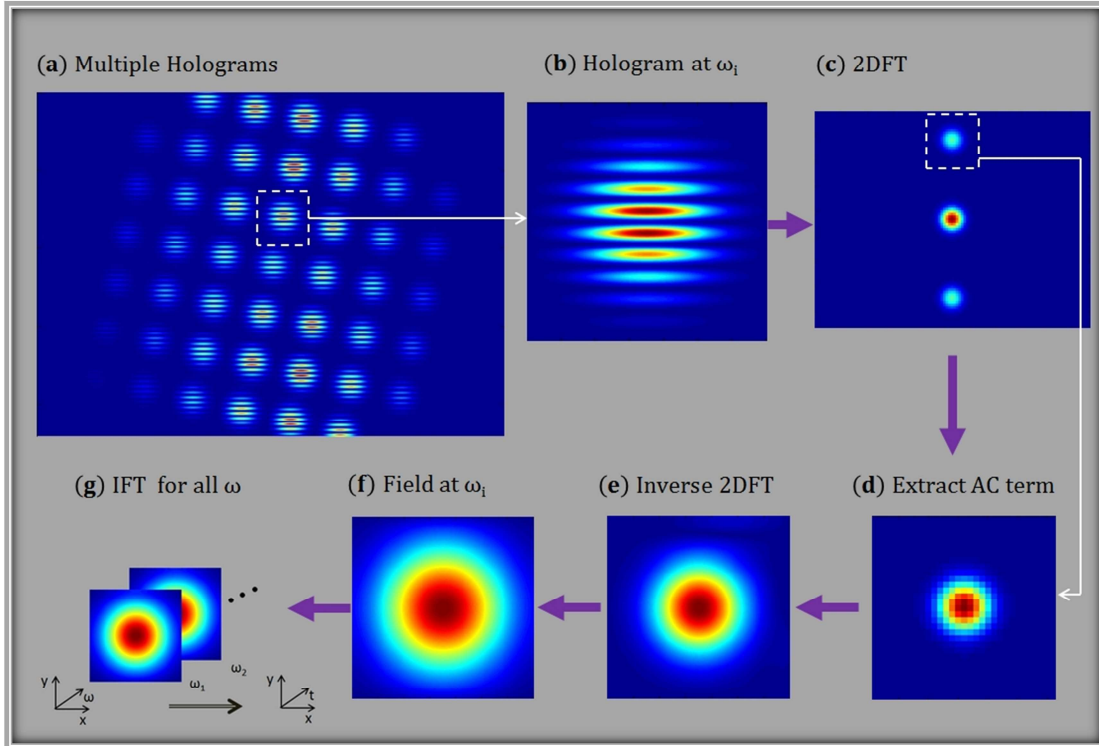


Figure 2. Illustration of the STRIPED FISH retrieval algorithm. Amplitudes are plotted for complex quantities. **a.** Multiple holograms of different frequencies are recorded on the camera. **b.** Hologram of a certain frequency  $\omega_i$  is selected. **c.** The two dimensional Fourier transform (2DFT) is taken over spatial dimensions. **d.** The oscillating AC term is extracted. **e.** The inverse 2DFT transforms into the space  $(x,y)$  domain, obtaining a product term. **f.** Dividing the reference field to obtain the unknown spatial field at  $\omega_i$ ,  $E_u(x,y,\omega_i)$ . **g.** Performing **a-f** for every hologram yields  $E_u(x,y,\omega)$ , then  $E_u(x,y,t)$  by an inverse Fourier transform (IFT) into the time domain.

In its initial demonstration [58], STRIPED FISH successfully measured simple temporally and spatially chirped pulses. But, as with any new device, the initial implementation of STRIPED FISH had limitations.

*Spectral range:* The transmitted central wavelength of an IBPF depends approximately linearly on the beam incidence angle. As a result, a STRIPED FISH device’s spectral range is limited by the range of beam angles impinging on the IBPF, which itself is limited by the range of angles generated by the DOE. In order to increase the device spectral range, for a given IBPF, a smaller feature size of the DOE, thus larger range of beam angles emerging from it, is required.

*Aberrations:* When the pairs of beams emerging from the DOE diverge more, severe aberrations (especially pincushion) arise due to off-axis propagation through simple lenses.

*Order inequality:* The various holograms had inherently highly unequal intensities (low orders were more intense) due to the usual order-dependent diffraction efficiency at the DOE. When the beam was attenuated enough that the central holograms did not saturate the camera, the peripheral holograms were very faint and had a low signal-to-noise ratio.

*Very bright central zero-order artifact:* The useful holograms were accompanied by a strong and useless central artifact, which overwhelmed adjacent holograms. This zero-order central-spike artifact[58] was due to the reflection from substrate of the DOE, which consisted of mostly transparent regions with small, square reflective coatings. An attempt to eliminate this artifact involved operating in reflection at Brewster's angle of the substrate. It effectively removed the central-spike artifact, but it also, unfortunately, introduced a weak "ghost" reflection from the back surface of the substrate [58]. Moreover, operating the subsequent imaging system at such an oblique angle (Brewster's angle) was vulnerable to off-axis misalignment and suffered from astigmatism.

*Display method for the measured pulse:* Finally, even the seemingly simple task of plotting the measured pulse proved quite challenging, due to the inherent data volume of both the intensity and phase vs.  $x$ ,  $y$ , and  $t$  (i.e., two four-dimensional graphs). Previously[59], to show the time evolution, we either suppressed a dimension or made movies by plotting the intensity and instantaneous frequency as a function of  $x$  and  $y$  and slowing time by  $\sim 14$  orders of magnitude. While these movies displayed simple chirped pulses well, the instantaneous frequency can, in practice, be highly unnatural in appearance: white regions of pulses (where all frequencies are present) display as green—a well-known fundamental problem of the instantaneous-frequency concept.

## **2. Accomplished Research**

### **I. Improved STRIPED FISH Device: Measuring the Chirped Pulse Beating**

#### **a. Improvements**

To address the problems, improvements are made. Firstly, we have converted to a normal incidence "negative DOE", whose transmission function is equal to the reflection function of the previous DOE. Therefore, this new grating has the same diffraction pattern in transmission, as before in reflection. But, as it works in a transmission manner, it has a no zero-order central-spike artifact or "ghost" reflection.

Secondly, we added an apodizing neutral density filter (ANDF), placed near the focal plane of the first lens (see Fig. 3a). Its radially decreasing optical density significantly attenuates central beams (low diffraction orders) relative to peripheral ones (high orders). As a result, it better balances the intensities of the various diffracted orders, as seen from Fig. 3b and 3d.

Thirdly, to collect the highly divergent beams and direct them to the camera without aberrations, we added an imaging system comprising two highly aberration-corrected commercial photographic lenses. Such lenses are designed for large incidence angles, as are common in photography. These lenses successfully image the divergent beams with minimal aberrations, allowing a greater range of angles at the IBPF and therefore a larger wavelength range (see Fig. 3c and 3d). Although these multi-element lenses contain significant amounts of glass, they can be used in our ultrafast-optical device because the

resulting group-delay dispersion is experienced by both the unknown and reference pulses and cancels out of the holographic measurement.

With these improvements, up to 40 holograms could be imaged onto a 10.5mm×7.73mm camera chip with negligible aberrations. It increased the spectral range and also allowed the device to use the full dynamic range of the camera (8 bits, 0 - 255) with a reasonable signal-to-noise ratio.

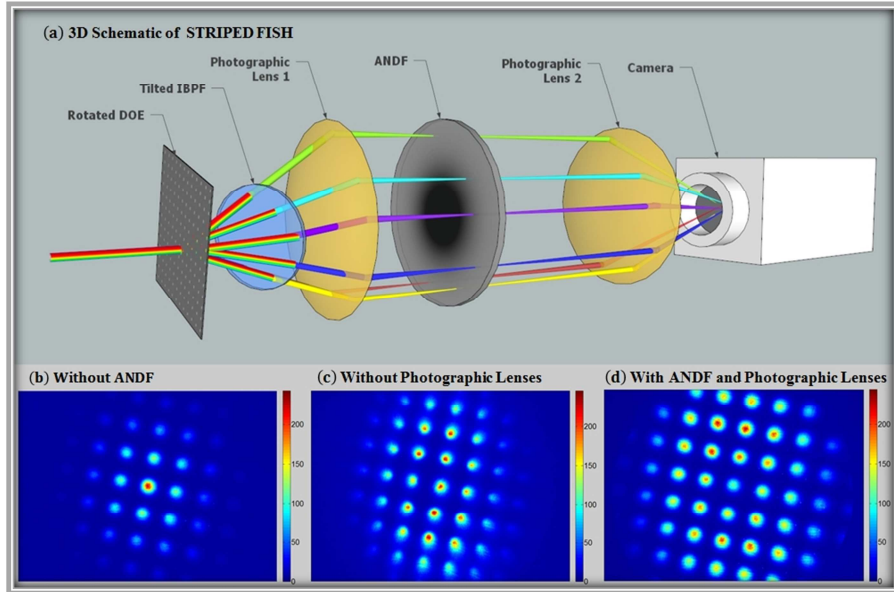


Figure 3. The improved STRIPED FISH apparatus and camera shots, showing the effect of the ANDF and photographic lenses, when only one beam is incident. **a.** 3D schematic of the STRIPED FISH apparatus. The input broadband beam is split into multiple quasi-monochromatic beams and then imaged onto the camera. **b.** Camera shot without the ANDF. Note that, due to the diffraction efficiencies and pulse spectrum, the central spot appears much brighter than the peripheral ones (27.3 times difference in peak intensity). **c.** Camera shot imaged by using two simple convex lenses. Note the aberrations introduced by the diverging beams. **d.** Camera shot after applying the ANDF and photographic lenses. Note the increased peripheral visibility (5.7 times peak intensity difference) and suppressed aberrations, resulting in a good signal-to-noise ratio for a wider range of wavelengths.

To more intuitively display the measured intensity and phase (vs.  $x$ ,  $y$ , and  $t$ ), we no longer use the instantaneous frequency and now instead compute numerical spectrograms of the retrieved pulse at each point in space using a variably delayed numerically generated gate pulse (a fraction of a pulse length long). The expression for these spectrograms is:

$$Sp(x, y, T, \omega) = \left| \int_{-\infty}^{\infty} E(x, y, t) g(t - T) \exp(-i\omega t) dt \right|^2$$

where  $g(t - T)$  is the numerical gate function with variable delay  $T$ .

We then compute overlap integrals of each spectrogram with red, green, and blue response functions:

$$R(x, y, T) = \int_{-\infty}^{\infty} Sp(x, y, T, \omega) R(\omega) d\omega$$

where  $R(\omega)$  is (for example) a red response function. This function is a simple Gaussian centered at a red frequency if true color is desired. If false color is desired, then this function is centered on the redder colors of the pulse spectrum. Similar response functions are used to compute the green (or center for false

color) and blue (or bluer) overlap integrals. The resulting color functions then serve as RGB values (vs.  $x$ ,  $y$  and  $t$ ), ensuring that a pixel appears white at places and times when the whole spectrum is present, and red/blue biased when longer/shorter wavelengths dominate. Also, we normalize the total color contents, so that the brightness (weight of color) represents the relative intensity (vs.  $x$ ,  $y$  and  $t$ ). Since the color of the pixels represents phase, both the intensity and phase information is contained in the RGB functions. This allows us to generate color movies as the human eye would perceive the pulse if the eye actually had the temporal resolution to do so.

### b. Experimental Setup

To demonstrate the effects of these improvements, we performed measurements on spatiotemporally complex pulses. We also used a high-rep-rate oscillator, so the measurements were not truly single shot, but we used only a single camera frame, yielding a proof of principle that true single-shot measurements are possible. As shown in Fig. 4, the output from a Ti:Sapphire oscillator (KMLabs, 800nm center wavelength, 20nm in FWHM), propagated through a pulse compressor (Swamp Optics BOA Compressor) and then through a spatial filter made of two convex lenses (first 300mm, second 100mm) and a pinhole (PH, 75 $\mu$ m). A flip mirror (FP) was then used to switch the beam path into the GRENOUILLE (Swamp Optics, model 8-50). When the flip mirror was flipped out of the beam, the beam propagated into two sets of beam-splitters (BS) that divided it into three replicas. One acted as the reference pulse, and the other two were combined at different angles with varying amounts of chirp and delay, creating a double-pulse with chirped-pulse beating that varied with spatial position. Two delay stages were used to synchronize the two unknown pulses and the reference.

The coarse DOE was made by photo-masking a soda lime substrate with a dark-field chrome coating, which comprised an array of transparent square windows (3 $\mu$ m $\times$ 3 $\mu$ m, 15 $\mu$ m spacing) that diffracted the beams into highly divergent ( $\sim$ 30 $^\circ$ ) beam arrays. The DOE was rotated slightly ( $\sim$ 10 $^\circ$ ) in the vertical plane to ensure that different beam replicas propagated at different horizontal angles. Then the beams were spectrally resolved by an IBPF (Semrock LL01-852, 3.2nm bandwidth, tilted by  $\sim$ 40 $^\circ$ ), with their center wavelength determined by their incidence angle. In this way, the whole spectrum of interest ( $\sim$ 775 to  $\sim$ 825nm) could be measured, with all frequencies calibrated by a fiber-coupled spectrometer (Ocean Optics HR4000). The imaging system consisted of two photographic lenses (lens 1: Computar c-mount 50mm, f1.8; lens 2: Computar c-mount 75mm, f1.4) and an ANDF (Edmund Optics 64386). After the imaging system, the unknown double pulses interfered with the reference pulses on the camera screen (PixeLINK PL-A781, 3000 $\times$ 2208 pixels, 3.5 $\mu$ m pixel pitch), forming  $\sim$ 40 quasi-monochromatic ( $\sim$ 5nm bandwidth) holograms at different frequencies.

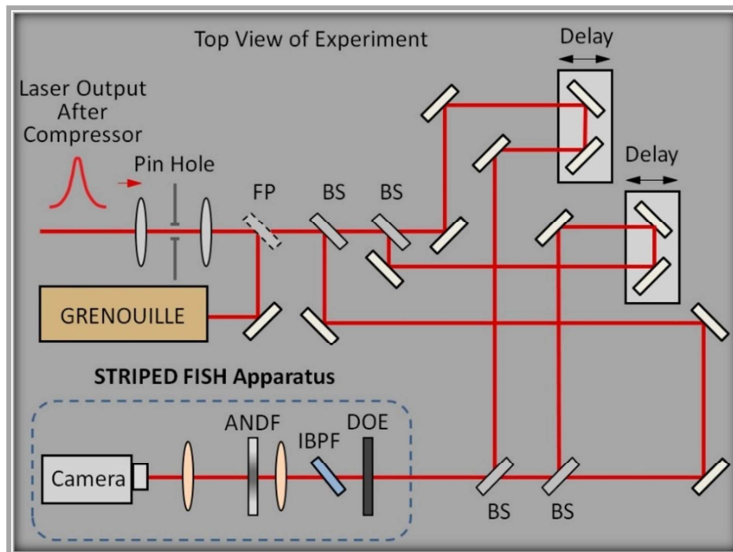




Figure 4. Top view of the current experiment for generating and measuring a complex unknown pulse consisting of two crossed, delayed, and chirped pulses. Chirp was controlled by the pulse compressor. A flip mirror (FP) was used to switch the beam to the GRENOUILLE. Three beam splitters (BS) provided the reference and double pulse to be measured. The STRIPED FISH device is shown within the dashed blue frame.

### c. Results and Simulations

Using the above setup, we measured spatiotemporally complex pulses consisting of double pulses crossed at various angles and with varying amounts of delay and chirp. Fig. 5a shows the resulting camera frame containing the multiple holograms generated by interference of the unknown and reference beams at different frequencies. Fig. 5b shows a camera image of only the unknown double pulse (with the reference beam blocked), yielding the spatial intensities for various frequencies  $I_u(x,y,\omega)$ . Fig. 5c and 5d show simulated camera frames, respectively for Fig. 5a and 5b, assuming Gaussian beams with the actual known beam-crossing angle, relative delay, pulse chirp, and spectral response parameters. A comparison shows that the measured camera frames agree well with what is expected based on our knowledge of the electric field.

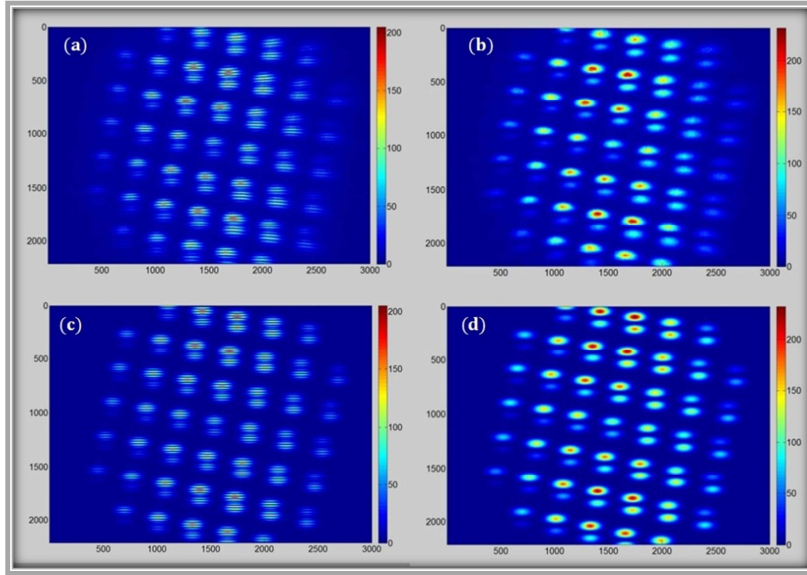


Figure 5. The STRIPED FISH traces and unknown pulse spectra for 28.9fs-spaced, 122.1fs-long positively chirped double pulses crossing at a small angle ( $\sim 0.1^\circ$ ).  $x$  and  $y$  axes are in pixels. **a.** Holograms created by interfering the reference and unknown double pulses on the camera screen. **b.** Blocking the reference pulse yields the unknown pulse spatial profiles for each frequency,  $I_u(x,y,\omega)$ . **c.** Simulated STRIPED FISH trace. **d.** Simulated unknown-pulse spatial profiles for each frequency,  $I_u(x,y,\omega)$ .

For each measurement, we generated a false-color STRIPED-FISH-measured movie of  $E_u(x,y,t)$ . The movie shows the spatially and temporally complex brightness and color patterns for the unknown crossing double pulses. Also, to ensure the credibility of our measured results, we have performed two crosschecks. The first check was a STRIPED FISH internal check: a STRIPED FISH measurement was performed for each individual pulse that made up the unknown double pulse, and then their retrieved electric fields were added numerically, using the known crossing angle and delay, to yield the unknown field. The double-pulse field (movie) obtained this way should be the same as the direct measurement of both pulses at once. A second check was to perform a theoretical simulation of the STRIPED FISH trace assuming simple Gaussian pulse and beam shapes and their known crossing angles and delays. Again, the

simulated movie is expected to have features similar to the directly measured one. As an example, three resulting movies from one such measurement are shown in Figure 6.

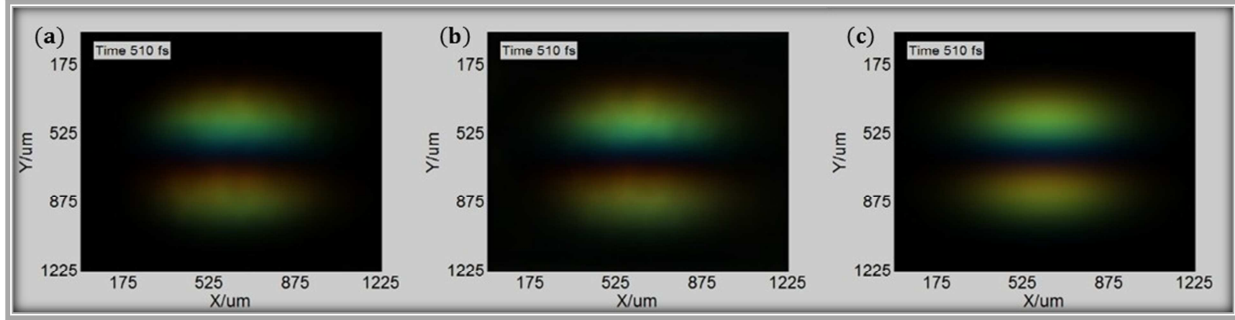


Figure 6. Movies of STRIPED FISH-measured interference between 28.9fs spaced, 122.1fs-long positively chirped double pulses crossing at a smaller angle. Relative time is shown in the upper left corner. **a.** Measured result (Media 1). **b.** Internal check result (Media 2). **c.** Simulation result (Media 3).

Since the exact delay between the pulses varies with spatial position due to the crossing angle, different colors experience constructive interference at different positions. As a result, the fringes move and change colors with time in interesting ways (shown by attached media).

## II. The STRIPED FISH Trace Catalog: Analyzing the Spatiotemporal Pulse Effects

### a. Transform-limited Pulse

To reveal the effects of spatiotemporal pulses on experimental STRIPED FISH traces, we perform a series of numerical simulations. Because the STRIPED FISH trace is generated by crossing the reference beam (which contains no STC) with the unknown beam at different frequencies, the trace itself reveals the spatio-spectral information of the unknown pulse. As shown in Table 1, the unknown pulse spatial structure is contained within each hologram: the spatial intensity is represented by the relative intensity distribution and the spatial phase by the fringe shape within one hologram. Likewise, the spectral information is reflected by multiple holograms: the spectral intensity is represented by the intensity variations and the spectral phase is indicated by the fringe shifts among different holograms.

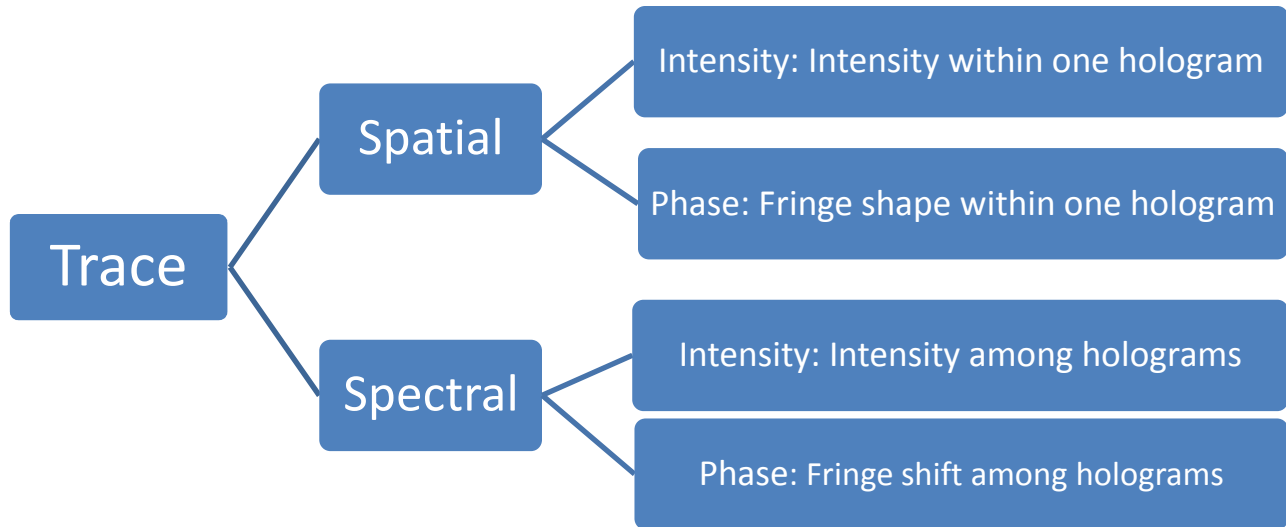


Table 1. The spatial and spectral effects of the unknown pulse on STRIPED FISH traces.

Firstly, as the simplest example, we investigate a transform-limited Gaussian pulse in both time and space. The expression for the spatiotemporal unknown field is:

$$E(x, y, t) = E(x, y) \times E(t) = \exp(-ax^2 - by^2) \times \exp(-ct^2)$$

The Fourier transform vs. time gives us the spatio-spectral field:

$$E(x, y, \omega) = E(x, y) \times E(\omega) = \sqrt{\frac{\pi}{c}} \exp(-ax^2 - by^2) \times \exp\left(-\frac{\omega^2}{4c}\right)$$

As  $a$ ,  $b$  and  $c$  are all real quantities ( $1\text{mm}^{-2}$ ,  $1\text{mm}^{-2}$  and  $1.76 \times 10^{-4} \text{fs}^{-2}$  respectively), the transform-limited pulse is collimated, and has no temporal chirp or STC. To emphasize the effects of the unknown pulse, we have made an assumption to plot the simulated trace more intuitively. That is, all of the holograms in the STRIEPD FISH will show the same intensity, when only the transform-limited reference pulse is incident. This is guaranteed practically by the imaging optics, which balances intensities of diffracted orders. Even if they are not exactly equal in experiment, people always can normalize them numerically after experimental trace is recorded. By assuming this, when the unknown pulse is also transform-limited, the STRIPED FISH trace will show equal-intensity holograms. For the purpose of illustration, 25 holograms are assigned with different wavelengths, ranging over 25nm, with central wavelength of 800nm. The STRIPED FISH trace of the transform-limited pulse is shown in Fig. 7, with color denoting the wavelength and brightness the intensity.

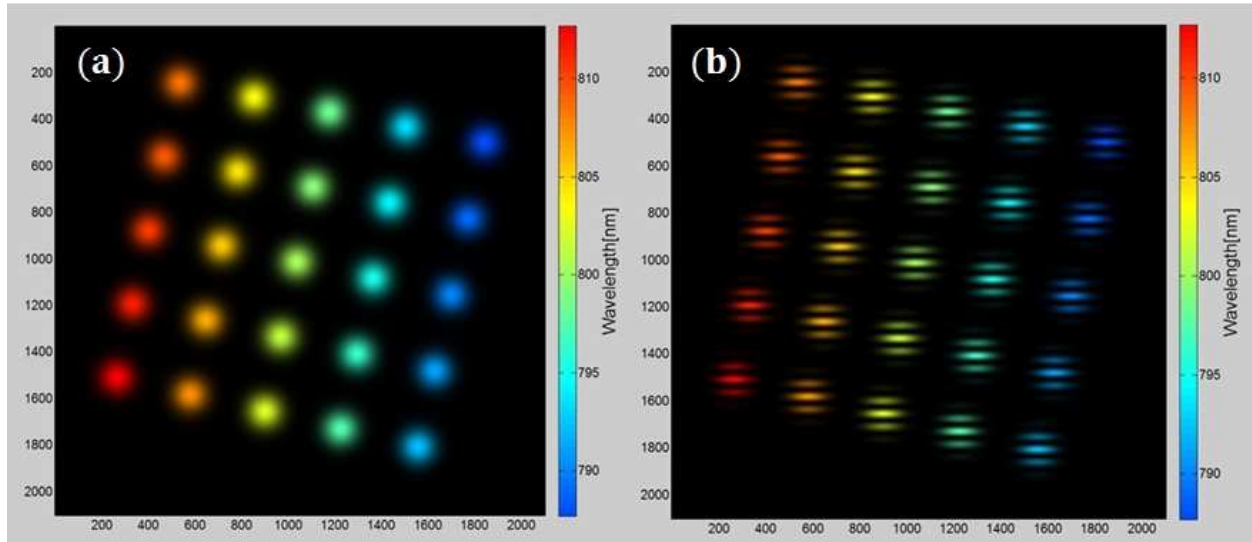


Figure 7. STRIPED FISH trace for Gaussian-shaped transform-limited pulse. Note that the holograms have equal intensities in different wavelengths, as indicated by their colors. **a.** Unknown pulse pattern. **b.** The STRIPED FISH holograms.  $x$  and  $y$  axes are in  $10\text{-}\mu\text{m}$  pixels.

### **b. Temporal and Spatial Double Pulses**

To better illustrate the effects in Table 1, we have simulated two more cases on temporal double pulses and spatial double pulses. The STRIPED FISH traces are shown in Figure 8.

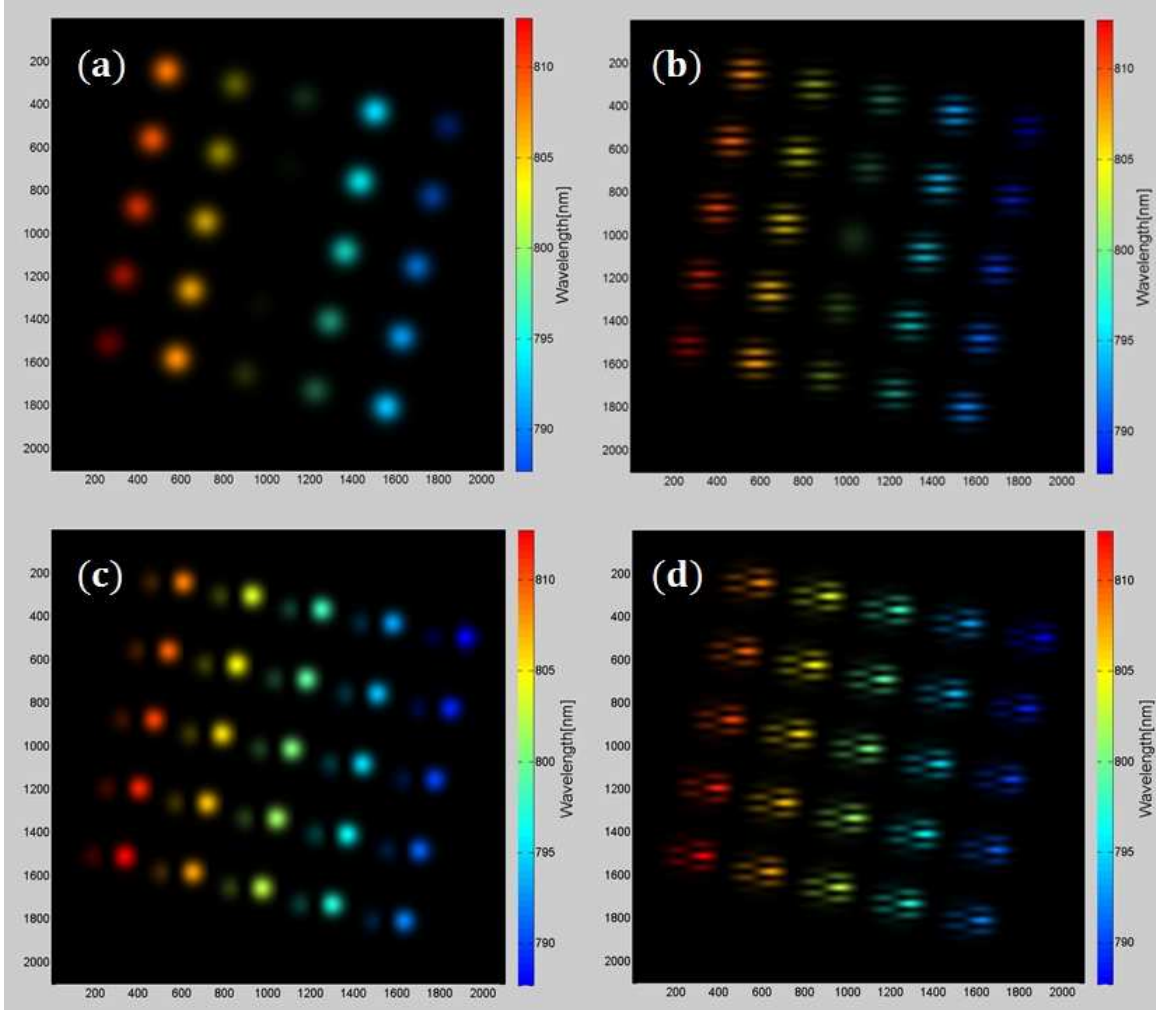


Figure 8. STRIPED FISH traces for double pulses. **a.** Pattern of the temporal double pulses, with equal intensities and  $\pi$  phase jump between the two component pulses. **b.** The STRIPED FISH holograms of the temporal double pulses. **c.** Pattern of the spatial double pulses, with the left pulse of one fourth intensity as the right pulse. A  $\pi$  phase jump is incorporated between the two pulses. **d.** The STRIPED FISH holograms of the spatial double pulses.

The temporal double pulses, each being transform-limited, share the same intensity. One pulse is delayed by  $\tau$  (136fs) from the other, with a  $\pi$  phase jump in between. To show their fringe variation, we set their arrival time to be  $t_0$  (209fs), so that spectrally they have a linearly varying phase. The expression of the unknown field is as below:

$$E(x, y, t) = \exp(-ax^2 - by^2) \times \exp[-c(t + t_0)^2] + \exp(i\pi) \times \exp(-ax^2 - by^2) \times \exp[-c(t + t_0 + \tau)^2]$$

From the trace (Fig. 8a and 8b), we can clearly see the spectral intensity variations between different holograms. Also, from their fringes shifting (compared with Fig. 7b) we know that the spectral phase of the unknown pulse is varying with respect to the reference pulse, which is distortion-free.

Similarly, we demonstrate the spatial effects by implementing a pair of spatial double pulses. Two spatial pulses are assumed to be propagating in the same direction, the left of which is half of the amplitude (therefore quarter intensity) as the right one. To show the spatial phase variation, we incorporate a  $\pi$  phase jump between the two component pulses. The expression is:

$$E(x, y, t) = \exp[-a(x - x_0)^2 - by^2] \times \exp(-ct^2) + 0.5 \times \exp(i\pi) \exp[-a(x + x_0)^2 - by^2] \times \exp(-ct^2)$$

As is obvious from Fig. 8c and 8d, the left pulse appears dimmer than the right one. Also, in the middle of each hologram, we can observe a fringe discontinuity due to the spatial phase jump.

### c. Spatiotemporally Coupled Pulses

Now we turn to see the effect of spatiotemporally coupled pulses on STRIPED FISH traces. To begin with, note that the STRIPED FISH trace presents itself in the spatial and spectral domain, we first look at two effects: the spatial chirp (SPC) and the wave-front tilt dispersion (WFD). These two STCs are the “fundamental” ones in the spatio-spectral domain [60]. The effect of SPC along x and y directions are similar, therefore only SPC along x is shown in Figure 9. The corresponding expression is:

$$E(x, y, \omega) = \exp(-ax^2 - by^2) \times \exp(2x\omega \times SPC) \times \exp\left(-\frac{\omega^2}{4 \times (-iTCP + c)}\right)$$

where  $SPC$  and  $TCP$  are the spatial chirp and temporal chirp ( $-4.57 \times 10^3$  fs/mm and  $-2.83 \times 10^{-4}$  fs<sup>-2</sup> respectively). As expected, in the figures, the spatial chirp causes different frequencies to shift in space linearly with their varying frequencies.

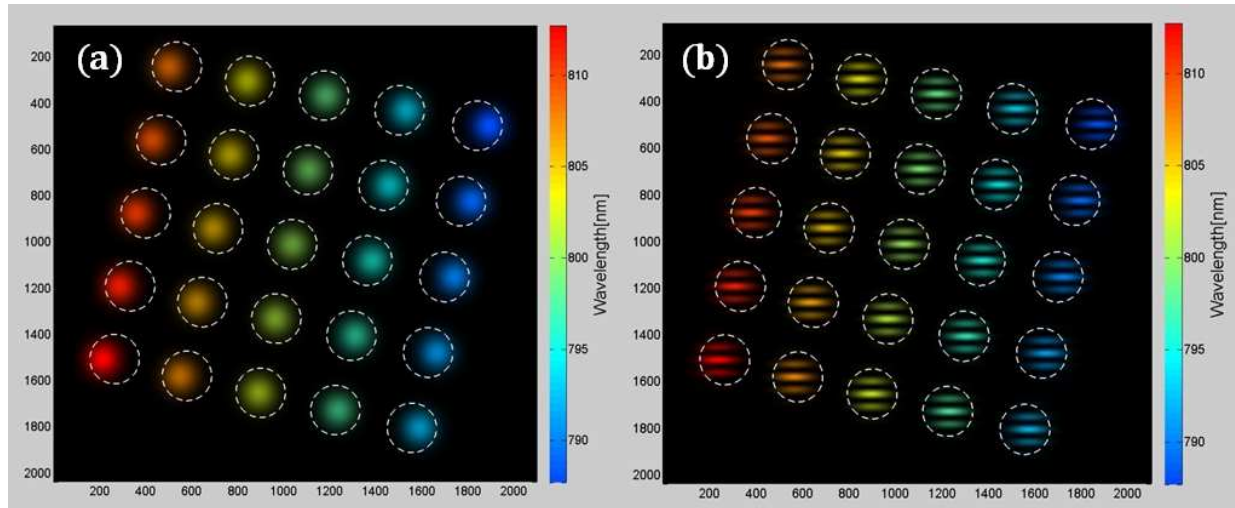


Figure 9. STRIPED FISH traces for unknown pulse with spatial chirp. The white circular contours mark the central positions when there is no STC. **a.** Patterns of spatially chirped pulse along x direction. **b.** The STRIPED FISH holograms.

Shown in Fig. 10a and 10b are traces for WFD ( $-1.14 \times 10^4$  fs/mm) along x and y, respectively. The pulse patterns are not plotted, because only the phase variation matters. As in the figures, the WFD along x causes the fringes to change their orientations; however, the WFD along y direction causes the spacing

between fringes to vary, increasing from red to blue. In both figures, center positions of the holograms are not shifted. The expressions for the WFD pulses are as below:

$$E(x, y, \omega) = \exp(-ax^2 - by^2) \times \exp(2ix\omega \times WFD) \times \exp\left(-\frac{\omega^2}{4 \times (-iTCP + c)}\right)$$

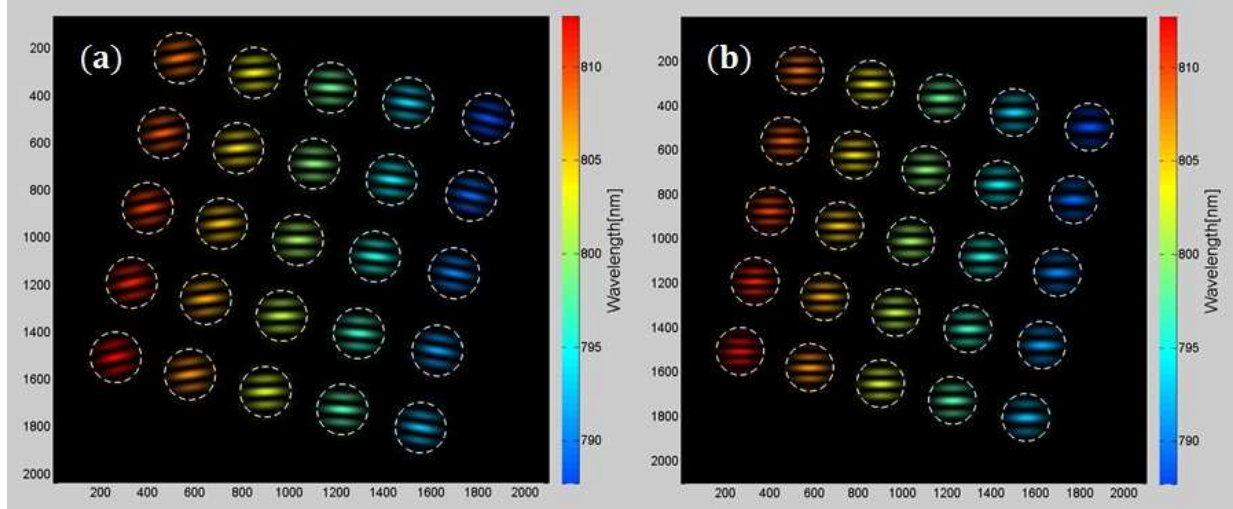


Figure 10. The STRIPED FISH traces for wave-front tilt dispersion. The white circular contours show the central positions when there is no STC. **a.** WFD along x. **b.** WFD along y.

Based on the “fundamental” cases, more complicated traces are investigated. For example, the STRIPED FISH trace of a pulse with pulse front tilt (PFT) along x direction is shown in Fig. 11a. From the figure, it is observed that the holograms have both effects from SPC (position shift along x) and WFD (fringe orientation rotation), as is explained in Ref [60]. In Fig. 11b, a STRIPED FISH trace of a focusing spatially chirped pulse is shown, from which frequency-shifted center positions and curved fringes can be observed.

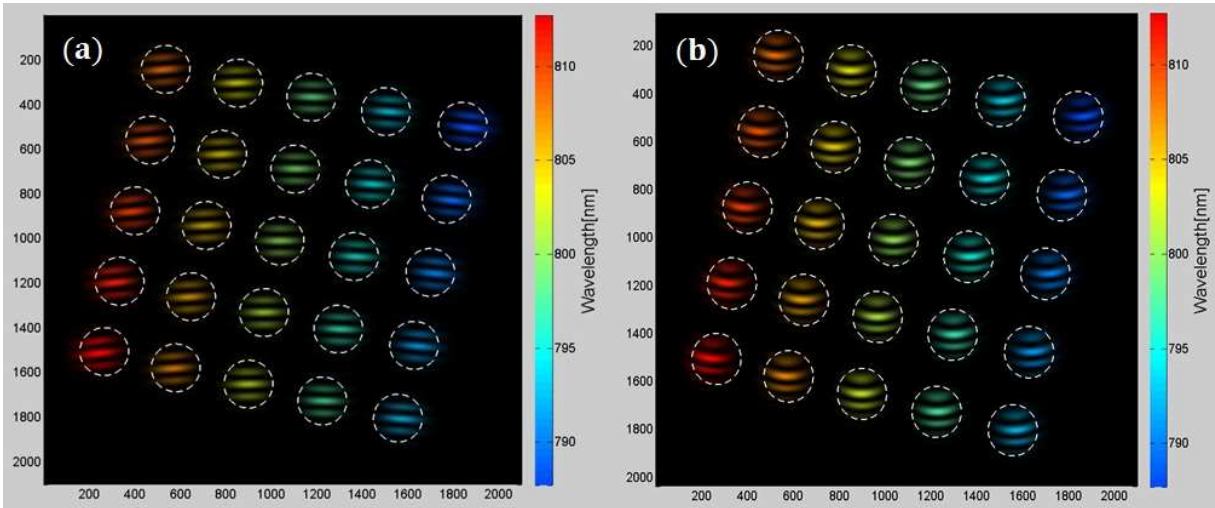


Figure 11. The STRIPED FISH traces for complicated STCs. The white circles shows the equal-intensity contours of the pulse with no STC. **a.** PFT along x. **b.** Focusing pulse with SPC along x.

### 3. Proposed Research

#### I. Measuring Interesting Spatiotemporal Pulses.

##### a. Ultrafast Lighthouse Effect

Other than the commonly-measured spatiotemporal effects, such as angular dispersion and pulse front tilt, in our recent work, we have identified another interesting first-order STC with the name of “ultrafast lighthouse effect”, where a light pulse or pulse train spirals outward like a beam emitted by a lighthouse (see Fig. 12)[33,60]. This very general effect opens the way to a new generation of attosecond light sources, particularly suitable for attosecond pump-probe experiments [61,62]. And it also provides a powerful new tool for ultrafast metrology, for instance, giving direct access to fluctuations in the phase of the laser field oscillations with respect to the pulse envelope (the so-called carrier-envelope relative phase), right at the focus of even the most intense ultrashort laser beams. STRIPED FISH, which measures the complete spatiotemporal intensity and phase, is extremely suitable for measuring the ultrafast lighthouse effect. Therefore, we propose to measure such effect with the femtosecond output from our Ti: Sapphire oscillator.

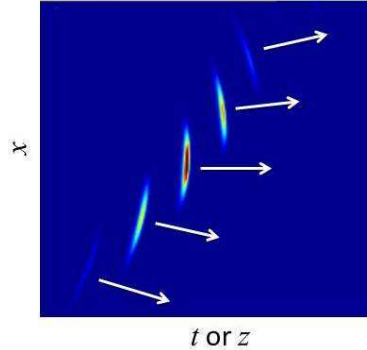


Fig. 12. Simulation of the ultrafast lighthouse effect, which holds promise for interesting attosecond applications. Arrows indicate propagation directions, and color indicates the pulse intensity [61].

##### b. Fiber Spatial Mode Measurement

The output from multi-mode fibers usually has more than one spatial mode. Actually, many applications, such as those in dispersion compensation and nonlinear optics [63,64], are taking advantage of this fact. Therefore, knowing the spatial mode distribution of the fiber output is important. More, as light in different fiber modes has different propagating speed (modal dispersion), the fiber output is also rich in temporal structures. Currently, methods on characterizing fiber output have been implemented, such as  $M^2$ ,  $S^2$ ,  $C^2$  and  $S^T$  [65-68]. However, only partial information is obtained. With STRIPED FISH, we believe, more complete spatiotemporal measurement of the fiber output could be achieved. Specifically, we are planning to couple the pulse from our Ti: Sapphire oscillator into a multi-mode fiber, then use STRIPED FISH to characterize the modal behavior of fiber output.

#### II. Measuring Amplified Pulses.

##### a. Single-shot Measurement of the Focusing Pulse from Regenerative Amplifier.

To our knowledge, technology that measures the spatiotemporal properties of high-power femtosecond lasers is badly needed in our community due to the many nonlinear-optical, intensity-dependent effects that occur as pulses propagate through many amplifiers. Therefore, we propose to measure intense focusing pulses with STRIPED FISH, using the output from the regenerative amplifier (Coherent Legend

Elite) in our lab. Instead of operating at the focus, to avoid damage, we can make measurements before it at “conjugate points”, where a small fraction of the pulse can be picked off from the main beam and is reasonably well considered to be identical to the main pulse. Then, pulse propagating algorithm could be applied based on diffraction integrals (see Fig. 13). In this way, we propose to perform the complete spatiotemporal characterization of ultra-intense near-IR femtosecond laser pulses on a single shot. Other than possible distortions in the pulse, we would also investigate the diffraction and aberration effects caused by the amplified pulses.

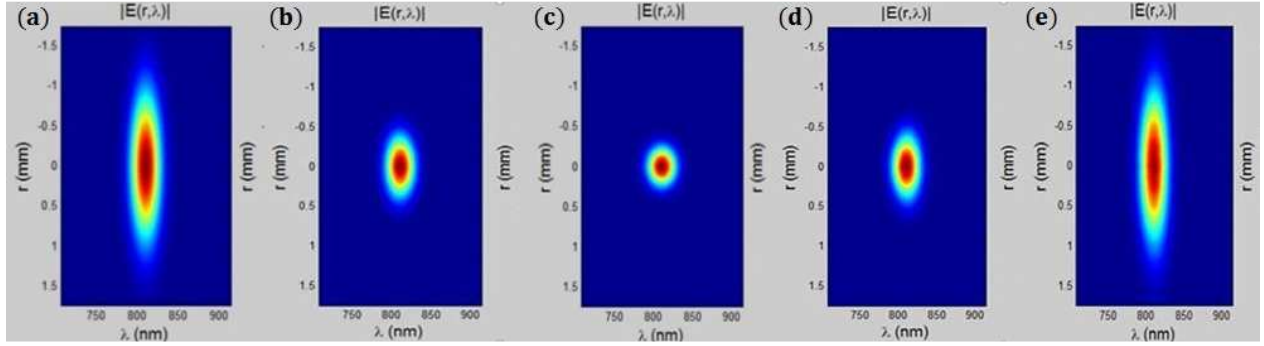


Figure 13. Propagation of the focusing pulse by calculating diffraction integrals. Spatio-spectral amplitudes are shown, as the  $z$  coordinate increases from **a** to **e**.

### b. Collaboration with the PHI Group to Measure the Super-intense Pulses

The Physics of High Intensity (PHI) group in Saclay, France studies the interaction of light and plasma, as well as laser-driven particle acceleration. Their main working tool is the UHI100 laser, a 100TW peak power, 20fs, 10Hz laser system, coupled to a radioactivity-protected experimental area. Despite their impressive present performance (thanks to the double plasma mirror [69,70]), several major improvements of ultrashort ultra-intense lasers are still required, e.g. the control of the STCs. STCs distort the beam badly in space and time and are clearly highly detrimental for the interaction of these lasers with matter. Indeed, they systematically decrease the peak light intensity at focus, by increasing both the pulse duration and the focal spot size. It is thus clearly essential to eliminate these couplings to achieve the highest possible intensities at focus, and thus maximize the energy of laser-accelerated particles. Therefore, we propose to use STRIPED FISH to characterize their laser output, revealing the spatiotemporal structure of the super-intense pulse.

## III. Measuring Nonlinear Optical Effects of Intense Pulses.

### a. Spectral Broadening and Self Focusing Effects

Nonlinear optical effects usually occur as a result of strong electric field, which is easily obtainable in amplified ultrashort pulses. The nonlinear phase effects, such as the self-phase modulation, could lead to spectral broadening of the pulse, which can be found useful in applications like broad band laser [71] and supercontinuum generation [72]. Also, spatially, the nonlinear phase would cause self-focusing, which usually is detrimental because it can cause damage due to the strong intensity at the focus. These effects are common in pulsed laser systems, and characterizing them would require both spatial and temporal measurement capability. Therefore, STRIPED FISH measurements would be helpful in understanding these nonlinear optical process.



## b. Filamentation Measurement

Another complex effect that is common in high-intensity pulses is called filamentation, in which light's nonlinear-optical effects compensate for both dispersive and diffractive effects, allowing the beam to propagate with the same small pulse length and beam size for many meters [73]. This effect is only partially understood, in part because it varies significantly from shot to shot due to its sensitivity to pulse fluctuations. While multi-shot measurements have been made, averaging over many pulses, true single-shot complete measurements are essential to its elucidation. One complication is that it is of very high intensity, and even a beam-splitter placed in the beam will be damaged by it. However, multiple grazing-incidence reflections can avoid damage to the beam-splitters and also reduce the intensity at the measurement device. These measurements should open the way to the ultimate optimization of these remarkable light sources, and to the accurate control of STCs in their applications, such as LIDAR and light-matter interactions [74,75]. By using our Coherent Legend Elite ultrafast amplified laser system, we can yield ~4mJ per pulse and pulses as short as ~40fs at 800nm at a repetition rate of 1kHz. Thus, we expect to generate filaments and use STRIPED FISH to characterize them.

## 4. Acknowledgement

This work is supported by the National Science Foundation, Grant #ECCS-1307817, and the Georgia Research Alliance. The author thanks Prof. Rick Trebino for his encouragement, knowledgeable guidance and great insight as an experimental scientist. Also, the author thanks Michelle Rhodes, Tsz Chun Wong, Dongjoo Lee and Saidur Rahaman for collaborations and helpful discussions. Some contents in this proposal are selected and paraphrased from the NSF grant proposal "*Single-shot Complete Spatiotemporal Measurement of Complex Light*" by Rick Trebino, and from a submission to Journal of the Optical Society of America B "*Simple Single-Frame Measurement of the Complete Spatiotemporal Field of a Complex Ultrashort Pulse*" by Zhe Guang, Michelle Rhodes, Matt Davis and Rick Trebino.

## 5. References

1. R. W. Boyd, Nonlinear optics (Academic press, 2003).
2. J. Goodman, Introduction to Fourier optics (Roberts and Company Publishers, 2008).
3. W. Demtröder, Laser spectroscopy: basic concepts and instrumentation (Springer, 2004).
4. R. Loudon, The quantum theory of light (Oxford university press, 2000).
5. A. Weiner, Ultrafast optics (John Wiley & Sons, 2011).
6. R. Thomson, C. Leburn, and D. T. Reid, Ultrafast Nonlinear Optics (Springer, 2013).
7. P. Hannaford, Femtosecond laser spectroscopy (springer, 2005).
8. R. Trebino, Frequency-Resolved Optical Gating: The Measurement of Ultrashort Laser Pulses (Kluwer Academic Publishers, 2002).
9. R. Trebino, K. W. DeLong, D. N. Fittinghoff, J. N. Sweetser, M. A. Krumbügel, and D. J. Kane, "Measuring Ultrashort Laser Pulses in the Time-Frequency Domain Using Frequency-Resolved Optical Gating," Review of Scientific Instruments 68, 3277-3295 (1997).
10. F. Quere, Y. Mairesse, and J. Itatani, "Temporal characterization of attosecond XUV fields," J. Modern Optics 52(2-3), 339-360 (2005).
11. K. Michelmann, T. Feurer, R. Fernsler, and R. Sauerbrey, "Frequency resolved optical gating in the UV using the electronic Kerr effect," Applied Physics B (Lasers and Optics) B63(5), 485-489 (1996).
12. P. Bownan and R. Trebino, "Complete single-shot measurement of arbitrary nanosecond laser pulses in time," Opt. Expr. 19(2), 1367-1377 (2011).
13. Y. Mairesse and F. Quéré, "Frequency-resolved optical gating for complete reconstruction of attosecond bursts," Phys Rev A 71, 011401 (2005).

14. J.-C. Chanteloup, E. Salmon, C. Sauteret, A. Migus, P. Zeitoun, A. Klisnick, A. Carillon, S. Hubert, D. Ros, and P. Nickles, "Pulse-front control of 15-TW pulses with a tilted compressor, and application to the subpicosecond traveling-wave pumping of a soft-x-ray laser," *JOSA B* 17, 151-157 (2000).
15. B. A. Richman, S. E. Bisson, R. Trebino, E. Sidick, and A. Jacobson, "All-prism achromatic phase matching for tunable second-harmonic generation," *Applied Optics* 38, 3316-3323 (1999).
16. T. C. Wong, and R. Trebino, "Single-frame measurement of complex laser pulses tens of picoseconds long using pulse-front tilt in cross-correlation frequency-resolved optical gating," *JOSA B* 30, 2781-2786 (2013).
17. V. Chauhan, P. Bowlan, J. Cohen, and R. Trebino, "Single-diffraction-grating and grism pulse compressors," *Journal of the Optical Society of America B* 27, 619-624 (2010).
18. F. Frei, A. Galler, and T. Feurer, "Space-time coupling in femtosecond pulse shaping and its effects on coherent control," *The Journal of chemical physics* 130, 034302 (2009).
19. S. Cundiff, E. Ippen, H. Haus, and W. Knox, "Frequency-dependent mode size in broadband Kerr-lens mode locking," *Optics Letters* 21, 662-664 (1996).
20. Z. Bor, "Distortion of femtosecond laser pulses in lenses and lens systems," *Journal of Modern Optics* 35, 1907-1918 (1988).
21. P. Bowlan, P. Gabolde, and R. Trebino, "Directly measuring the spatio-temporal electric field of focusing ultrashort pulses," *Opt. Expr.* 15, 10219-10230 (2007).
22. M. Kempe, and W. Rudolph, "Femtosecond pulses in the focal region of lenses," *Physical Review A* 48, 4721 (1993).
23. J. Jasapara, and W. Rudolph, "Characterization of sub-10-fs pulse focusing with high-numerical-aperture microscope objectives," *Optics Letters* 24, 777-779 (1999).
24. H. Kumagai, S.-H. Cho, K. Ishikawa, K. Midorikawa, M. Fujimoto, S.-i. Aoshima, and Y. Tsuchiya, "Observation of the complex propagation of a femtosecond laser pulse in a dispersive transparent bulk material," *JOSA B* 20, 597-602 (2003).
25. A. Matijošius, P. Di Trapani, A. Dubietis, R. Piskarskas, A. Varanavičius, and A. Piskarskas, "Nonlinear space-time dynamics of ultrashort wave packets in water," *Optics Letters* 29, 1123-1125 (2004).
26. D. Faccio, M. A. Porras, A. Dubietis, F. Bragheri, A. Couairon, and P. Di Trapani, "Conical emission, pulse splitting, and X-wave parametric amplification in nonlinear dynamics of ultrashort light pulses," *Physical Review Letters* 96, 193901 (2006).
27. A. Couairon, and A. Mysyrowicz, "Femtosecond filamentation in transparent media," *Physics reports* 441, 47-189 (2007).
28. D. E. Adams, T. A. Planchon, A. Hrin, J. A. Squier, and C. G. Durfee, "Characterization of coupled nonlinear spatio-spectral phase following an ultrafast self-focusing interaction," *Optics Letters* 34, 1294-1296 (2009).
29. P. O'Shea, M. Kimmel, X. Gu, and R. Trebino, "Highly simplified device for ultrashort-pulse measurement," *Optics Letters* 26, 932-934 (2001).
30. S. Akturk, M. Kimmel, P. O'Shea, and R. Trebino, "Extremely simple device for measuring 20-fs pulses," *Opt. Lett.* 29, 1025-1027 (2004).
31. S. Akturk, M. Kimmel, P. O'Shea, and R. Trebino, "Measuring spatial chirp in ultrashort pulses using single-shot Frequency-Resolved Optical Gating," *Opt. Expr.* 11, 68-78 (2003).
32. S. Akturk, M. Kimmel, P. O'Shea, and R. Trebino, "Measuring pulse-front tilt in ultrashort pulses using GRENOUILLE," *Opt. Expr.* 11, 491-501 (2003).
33. S. Akturk, X. Gu, P. Bowlan, and R. Trebino, "Spatio-temporal couplings in ultrashort laser pulses," *Journal of Optics* 12, 093001 (2010).
34. I. A. Walmsley, and C. Dorrer, "Characterization of ultrashort electromagnetic pulses," *Advances in Optics and Photonics* 1, 308-437 (2009).
35. F. Bragheri, D. Faccio, F. Bonaretti, A. Lotti, M. Clerici, O. Jedrkiewicz, C. Liberale, S. Henin, L. Tartara, and V. Degiorgio, "Complete retrieval of the field of ultrashort optical pulses using the angle-frequency spectrum," *Optics Letters* 33, 2952-2954 (2008).
36. S. Kahaly, S. Monchocé, V. Gallet, O. Gobert, F. Réau, O. Tcherbakoff, P. D'Oliveira, P. Martin, and F. Quéré, "Investigation of amplitude spatio-temporal couplings at the focus of a 100 TW-25 fs laser," *Applied Physics Letters* 104, 054103 (2014).
37. C. Dorrer, E. Kosik, and I. Walmsley, "Direct space time-characterization of the electric fields of ultrashort optical pulses," *Optics Letters* 27, 548-550 (2002).

38. C. Dorrer, E. Kosik, and I. Walmsley, "Spatio-temporal characterization of the electric field of ultrashort optical pulses using two-dimensional shearing interferometry," *Applied Physics B* 74, s209-s217 (2002).
39. L. Gallmann, G. Steinmeyer, D. Sutter, T. Rupp, C. Iaconis, I. Walmsley, and U. Keller, "Spatially resolved amplitude and phase characterization of femtosecond optical pulses," *Optics Letters* 26, 96-98 (2001).
40. A. S. Wyatt, I. A. Walmsley, G. Stibenz, and G. Steinmeyer, "Sub-10 fs pulse characterization using spatially encoded arrangement for spectral phase interferometry for direct electric field reconstruction," *Optics Letters* 31, 1914-1916 (2006).
41. E. M. Kosik, A. S. Radunsky, I. A. Walmsley, and C. Dorrer, "Interferometric technique for measuring broadband ultrashort pulses at the sampling limit," *Optics Letters* 30, 326-328 (2005).
42. F. Bonaretti, D. Faccio, M. Clerici, J. Biegert, and P. Di Trapani, "Spatiotemporal amplitude and phase retrieval of Bessel-X pulses using a Hartmann-Shack sensor," *Optics Express* 17, 9804-9809 (2009).
43. E. Rubino, D. Faccio, L. Tartara, P. K. Bates, O. Chalus, M. Clerici, F. Bonaretti, J. Biegert, and P. Di Trapani, "Spatiotemporal amplitude and phase retrieval of space-time coupled ultrashort pulses using the Shackled-FROG technique," *Optics Letters* 34, 3854-3856 (2009).
44. S. L. Cousin, J. M. Bueno, N. Forget, D. R. Austin, and J. Biegert, "Three-dimensional spatiotemporal pulse characterization with an acousto-optic pulse shaper and a Hartmann-Shack wavefront sensor," *Optics Letters* 37, 3291-3293 (2012).
45. C. Hauri, J. Biegert, U. Keller, B. Schaefer, K. Mann, and G. Marowski, "Validity of wave-front reconstruction and propagation of ultrabroadband pulses measured with a Hartmann-Shack sensor," *Optics Letters* 30, 1563-1565 (2005).
46. W. Amir, T. A. Planchon, C. G. Durfee, J. A. Squier, P. Gabolde, R. Trebino, and M. Müller, "Simultaneous visualization of spatial and chromatic aberrations by 2D Fourier Transform Spectral Interferometry," *Opt. Lett.* 31, 2927 (2006).
47. W. Amir, T. Planchon, C. Durfee, and J. Squier, "Complete characterization of a spatiotemporal pulse shaper with two-dimensional Fourier transform spectral interferometry," *Optics Letters* 32, 939-941 (2007).
48. P. Bownan, P. Gabolde, A. Shreenath, K. McGresham, R. Trebino, and S. Akturk, "Crossed-beam spectral interferometry: a simple, high-spectral-resolution method for completely characterizing complex ultrashort pulses in real time," *Opt. Expr.* 14, 11892 (2006).
49. B. Alonso, Í. J. Sola, Ó. Varela, J. Hernández-Toro, C. Méndez, J. San Román, A. Zaïr, and L. Roso, "Spatiotemporal amplitude-and-phase reconstruction by Fourier-transform of interference spectra of high-complex-beams," *JOSA B* 27, 933-940 (2010).
50. F. Eilenberger, A. Brown, S. Minardi, and T. Pertsch, "Imaging cross-correlation FROG: measuring ultrashort, complex, spatiotemporal fields," *Optics Express* 21, 25968-25976 (2013).
51. J. Trull, O. Jedrkiewicz, P. Di Trapani, A. Matijosius, A. Varanavicius, G. Valiulis, R. Danielius, E. Kucinskas, A. Piskarskas, and S. Trillo, "Spatiotemporal three-dimensional mapping of nonlinear X waves," *PHYSICAL REVIEW-SERIES E*- 69, 026607-026607 (2004).
52. B. Alonso, I. Sola, O. Varela, C. Méndez, I. Arias, J. San Román, A. Zaïr, and L. Roso, "Spatio-temporal characterization of laser pulses by spatially resolved spectral interferometry," *Opt. Pura Apl* 43 (2010).
53. N. Mehta, C. Yang, Y. Xu, and Z. Liu, "Characterization of the spatiotemporal evolution of ultrashort optical pulses using FROG holography," *Optics Express* 22, 11099-11106 (2014).
54. P. Gabolde, and R. Trebino, "Single-shot measurement of the full spatiotemporal field of ultrashort pulses with multispectral digital holography," *Opt. Expr.* 14, 11460 (2006).
55. M. Bass, E. W. Van Stryland, D. R. Williams, and W. L. Wolfe, "Handbook of Optics. Fundamentals, Techniques, and Design, Vol. 1," I (1995).
56. P. Lissberger, and W. Wilcock, "Properties of all-dielectric interference filters. II. Filters in parallel beams of light incident obliquely and in convergent beams," *JOSA* 49, 126-128 (1959).
57. M. Takeda, H. Ina, and S. Kobayashi, "Fourier-transform method of fringe-pattern analysis for computer-based topography and interferometry," *J. Opt. Soc. Am.* 72, 156-160 (1982).
58. P. Gabolde, and R. Trebino, "Single-frame measurement of the complete spatio-temporal intensity and phase of ultrashort laser pulse(s) using wavelength-multiplexed digital holography," *J. Opt. Soc. Am. B* 25, A25-A33 (2008).
59. P. Gabolde, and R. Trebino, "Self-referenced measurement of the complete electric field of ultrashort pulses," *Opt. Expr.* 12, 4423 - 4429 (2004).

60. S. Akturk, X. Gu, P. Gabolde, and R. Trebino, "The general theory of first-order spatio-temporal distortions of Gaussian pulses and beams," *Opt. Express* 13, 8642–8661 (2005).
61. H. Vincenti and F. Quéré, "Attosecond Lighthouses: How To Use Spatiotemporally Coupled Light Fields To Generate Isolated Attosecond Pulses," *Phys. Rev. Lett.* 108, 113904 (2012)
62. J. Wheeler, A. Borot, S. Monchoce, H. Vincenti, A. Ricci, A. Malvache, R. Lopez-Martens and F. Quere, "Attosecond lighthouses from plasma mirrors," *Nature Photonics* 6, 829–833 (2012)
63. C. Poole, J. M. Wiesenfeld, D. J. Digiovanni, and A. M. Vengsarkar, "Optical fiber-based dispersion compensation using higher order modes near cutoff," *Lightwave Technology, Journal of* 12, 1746-1758 (1994).
64. J. Nicholson, J. Fini, A. Yablon, P. Westbrook, K. Feder, and C. Headley, "Demonstration of bend-induced nonlinearities in large-mode-area fibers," *Optics Letters* 32, 2562-2564 (2007).
65. A. E. Siegman, "Defining, measuring, and optimizing laser beam quality," in *Proc. SPIE*, 1868, 2–12. (1993)
66. J. Nicholson, A. Yablon, J. Fini, and M. Mermelstein, "Measuring the Modal Content of Large-Mode-Area Fibers", *IEEE JSTQE* 15 61-70 (2009).
67. D. N. Schimpf, R. A. Barankov, and S. Ramachandran, "Cross-correlated (C2) imaging of fiber and waveguide modes," *Opt. Express* 19(4) 13008-13019 (2011)
68. J. A. Carpenter, B. J. Eggleton, and J. Schroeder, "Spatially and temporally resolved imaging of modal content in photonic-bandgap fiber," in *CLEO: 2014, OSA Technical Digest (online)* (Optical Society of America, 2014), paper STu3N.2.
69. C. Thaury, F. Quere, J. P. Geindre, A. Levy, T. Ceccotti, P. Monot, M. Bougeard, F. Reau, P. d'Oliveira, P. Audebert, R. Marjoribanks, and P. Martin, "Plasma mirrors for ultrahigh-intensity optics," *Nat Phys* 3(6), 424-429 (2007).
70. C. Thaury, H. George, F. Quere, R. Loch, J. P. Geindre, P. Monot, and P. Martin, "Coherent dynamics of plasma mirrors," *Nat Phys* 4(8), 631-634 (2008).
71. M. Bache and B. Zhou, "High-energy pulse compressor using self-defocusing spectral broadening in anomalously dispersive media," in *CLEO: 2014, OSA Technical Digest (online)* (Optical Society of America, 2014), paper SW1E.7.
72. R. Alfano, and S. Shapiro, "Observation of self-phase modulation and small-scale filaments in crystals and glasses," *Physical Review Letters* 24, 592 (1970).
73. A. Braun, G. Korn, X. Liu, D. Du, J. Squier, and G. Mourou, "Self-channeling of high-peak-power femtosecond laser pulses in air," *Optics Letters* 20, 73-75 (1995).
74. P. Rairoux, H. Schillinger, S. Niedermeier, M. Rodriguez, F. Ronneberger, R. Sauerbrey, B. Stein, D. Waite, C. Wedekind, and H. Wille, "Remote sensing of the atmosphere using ultrashort laser pulses," *Applied Physics B* 71, 573-580 (2000).
75. W. Watanabe, T. Tamaki, Y. Ozeki, and K. Itoh, "Filamentation in ultrafast laser material processing," in *Progress in Ultrafast Intense Laser Science VI*(Springer, 2010), pp. 161-181.